



HHS Public Access

Author manuscript

Nat Struct Mol Biol. Author manuscript; available in PMC 2024 February 26.

Published in final edited form as:

Nat Struct Mol Biol. 2023 June ; 30(6): 735–739. doi:10.1038/s41594-023-00951-7.

Structural basis for Ca_vα₂δ:gabapentin binding

Zhou Chen^{1,6}, Abhisek Mondal^{1,6}, Daniel L. Minor Jr^{1,2,3,4,5,✉}

¹Cardiovascular Research Institute, University of California, San Francisco, CA, USA.

²Departments of Biochemistry and Biophysics, and Cellular and Molecular Pharmacology, University of California, San Francisco, CA, USA.

³California Institute for Quantitative Biomedical Research, University of California, San Francisco, CA, USA.

⁴Kavli Institute for Fundamental Neuroscience, University of California, San Francisco, CA, USA.

⁵Molecular Biophysics and Integrated Bio-imaging Division, Lawrence Berkeley National Laboratory, Berkeley, CA, USA.

⁶These authors contributed equally: Zhou Chen, Abhisek Mondal.

Abstract

Gabapentinoid drugs for pain and anxiety act on the Ca_vα₂δ-1 and Ca_vα₂δ-2 subunits of high-voltage-activated calcium channels (Ca_v1s and Ca_v2s). Here we present the cryo-EM structure of the gabapentin-bound brain and cardiac Ca_v1.2/Ca_vβ₃/Ca_vα₂δ-1 channel. The data reveal a binding pocket in the Ca_vα₂δ-1 dCache1 domain that completely encapsulates gabapentin and define Ca_vα₂δ isoform sequence variations that explain the gabapentin binding selectivity of Ca_vα₂δ-1 and Ca_vα₂δ-2.

Gabapentin (GBP) (1-(aminomethyl)cyclohexane acetic acid; Neurontin)¹ and the related gabapentinoid drugs pregabalin (Lyrica)^{2,3} and mirogabalin (Tarlige)^{4,5} are widely used to treat post-herpetic neuralgia, diabetic neuropathy, fibromyalgia, epilepsy, restless leg syndrome and generalized anxiety disorder. These drugs bind to high-voltage-activated

✉ **Correspondence and requests for materials** should be addressed to Daniel L. Minor. daniel.minor@ucsf.edu.

Author contributions

Z.C., A.M. and D.L.M. conceived the study and designed the experiments. Z.C. expressed and characterized the samples. Z.C. and A.M. collected and analyzed the cryo-EM data. Z.C. and A.M. built and refined the atomic models. D.L.M. analyzed data and provided guidance and support. Z.C., A.M. and D.L.M. wrote the paper.

Competing interests

The authors declare no competing interests.

Reporting summary

Further information on research design is available in the Nature Portfolio Reporting Summary linked to this Article.

Additional information

Extended data is available for this paper at <https://doi.org/10.1038/s41594-023-00951-7>.

Peer review information *Nature Structural & Molecular Biology* thanks Rachelle Gaudet and the other, anonymous, reviewer(s) for their contribution to the peer review of this work. Primary Handling Editor: Katarzyna Ciazynska, in collaboration with the *Nature Structural & Molecular Biology* team. Peer reviewer reports are available.

Reprints and permissions information is available at www.nature.com/reprints.

Supplementary information The online version contains supplementary material available at <https://doi.org/10.1038/s41594-023-00951-7>.

calcium channel (Ca_V) Ca_Vα₂δ-1 and Ca_Vα₂δ-2 subunits^{3,4,6–8}, but not to the related Ca_Vα₂δ-3 and Ca_Vα₂δ-4 isoforms^{2,9,10}. Gabapentinoid binding to Ca_Vα₂δ-1 and Ca_Vα₂δ-2 is thought to affect neuronal excitability by impairing Ca_V surface membrane expression^{3,7,8} through a mechanism involving Rab11a endosomal recycling^{11,12}. Although the GBP-binding site has been identified¹³, structural details of Ca_Vα₂δ:GBP interactions have not yet been defined.

High-voltage-gated calcium channels (Ca_V1 and Ca_V2)^{14,15} are multi-subunit voltage-gated ion channels comprising three key components—the pore-forming Ca_Vα₁ (refs. 14,15), cytoplasmic Ca_Vβ (ref. 16) and extracellular Ca_Vα₂δ (refs. 1,17) subunits. Recent cryo-EM structural studies of the Ca_V1.2/Ca_Vβ₃/Ca_Vα₂δ-1 channel complex¹³ revealed a Ca_Vα₂δ-1-bound L-leucine, a known Ca_Vα₂δ ligand^{1,18,19} and GBP competitor^{1,20}, that identified the gabapentinoid binding site^{1,17}. In this Brief Communication we present the 3.1-Å cryo-EM structure of the Ca_V1.2/Ca_Vβ₃/Ca_Vα₂δ-1 channel bound to GBP. The data show that GBP occupies the L-Leu binding site¹³ in the first subdomain of the Ca_Vα₂δ-1 dCache1 (Ca²⁺ channel and chemotaxis receptor) domain²¹. Structural analysis identifies six binding-site residues that differ between the GBP-sensitive isoforms, Ca_Vα₂δ-1 and Ca_Vα₂δ-2 (refs. 3,4,6–8), and the GBP-insensitive isoforms, Ca_Vα₂δ-3 and Ca_Vα₂δ-4 (refs. 2,9,10). These yield steric clashes with GBP and cause binding-site polarity changes that rationalize the GBP-insensitivity of the Ca_Vα₂δ-3 and Ca_Vα₂δ-4 isoforms.

Structure determination of a recombinant Ca_V1.2(C)/Ca_Vβ₃/Ca_Vα₂δ-1 channel complex¹³ comprising a version of human Ca_V1.2 truncated after the IQ domain (Ca_V1.2(C), 186 kDa) having wild-type functional properties¹³, rabbit Ca_Vβ₃ (54 kDa) and rabbit Ca_Vα₂δ-1 (125 kDa) in the presence of 11.7 mM GBP revealed a tripartite channel assembly (~370 kDa) (Fig. 1a) at an overall resolution of 3.1 Å (Extended Data Figs. 1 and 2a–c, and Table 1) largely similar to the L-Leu bound structure¹³ (root-mean-square deviation, r.m.s.d._{Ca} = 0.749 Å). As previously observed¹³, the sample also contained a chaperone:channel complex of the endoplasmic reticulum (ER) membrane protein complex (EMC)^{22–24}, Ca_V1.2(C) and Ca_Vβ₃ (Extended Data Figs. 1 and 2d,e). The overall structure of the Ca_V1.2(C)/Ca_Vβ₃/Ca_Vα₂δ-1:GBP complex is similar to other Ca_V1 and Ca_V2 structures^{13,25–27}. Ca_Vα₂δ-1 has a multi-domain architecture built from two double Cache domains²⁸, dCache1 and dCache2, and a von Willebrand factor type A (VWA) domain^{25,28,29} (Fig. 1a and Extended Data Fig. 3a). Importantly, the high Ca_Vα₂δ-1 local resolution (2.0–2.5 Å) and map quality (Fig. 1b–d and Extended Data Figs. 2b,c and 3a–f) allowed detailed comparison of the dCache1 domain with the L-Leu bound structure¹³. A map comparison (Fig. 1b–d and Supplementary Video 1) showed clear differences in the binding pocket density. These included a shape not present in the L-Leu bound maps (Fig. 1b–d) that had features that could be attributed to the GBP cyclohexyl ring and that defined the GBP-binding site.

Similar to L-Leu, GBP occupies a pocket in the first Ca_Vα₂δ-1 dCache1 β-barrel lined by Trp207, Val209, Tyr219, Trp225, Tyr238, Arg243, Trp245, Tyr452, Asp454, Ala455, Leu456, Thr463 and Asp493 (Fig. 1e and Extended Data Fig. 3f) that is closed to solvent access. In line with the similar affinities of the two ligands¹⁸, there are no large conformational differences in the dCache1 binding site relative to the Ca_Vα₂δ-1:L-Leu complex (r.m.s.d._{Ca} = 0.155 Å; Extended Data Fig. 4a). The structure shows that GBP

and $\text{Ca}_V\alpha_2\delta$ -2^{3,4,6-8}) and gabapentinoid-insensitive ($\text{Ca}_V\alpha_2\delta$ -3 and $\text{Ca}_V\alpha_2\delta$ -4, refs. 2,9,10) $\text{Ca}_V\alpha_2\delta$ isoforms (Fig. 2a). Mapping these on the $\text{Ca}_V\alpha_2\delta$ -1:GBP structure (Fig. 2b) reveals numerous alterations expected to interfere with GBP binding to $\text{Ca}_V\alpha_2\delta$ -3 and $\text{Ca}_V\alpha_2\delta$ -4, including (1) loss of a hydrogen-bond donor to the GBP carboxylate (Y238F), (2) introduction of steric clashes (V209Y, A217F³⁵ and A455S), two of which (V209Y and A217F) would occupy the same space as the GBP cyclohexyl ring, and (3) changes in contact residue size (Y219I) and polarity (Y219Q, L456Q and A455S) that reshape binding pocket physicochemical characteristics. The $\text{Ca}_V\alpha_2\delta$ -related protein CACHD1 also lacks most of the key GBP-binding residues (Fig. 2a), indicating that the effects of this protein on Ca_V surface expression³⁶ are likely to be GBP-independent. Taken together, the multiple changes between the GBP-sensitive and GBP-insensitive isoforms that remove hydrogen bonds, introduce steric clashes and reduce the hydrophobicity of the binding pocket provide a structural rationalization for the differences in gabapentinoid binding properties among the $\text{Ca}_V\alpha_2\delta$ isoforms^{2-4,7-10}.

Binding of GBP and gabapentinoids to the $\text{Ca}_V\alpha_2\delta$ subunit of Ca_V s is critical for the pharmacological effects of this drug class^{3,31-33}. The structural identity of the L-Leu¹³ and GBP-bound $\text{Ca}_V\alpha_2\delta$ complexes (Extended Data Fig. 4a) suggests that the effects of GBP on Ca_V function may arise from changes in the dynamic behavior of $\text{Ca}_V\alpha_2\delta$ when it is bound to different ligands. Structural definition of the $\text{Ca}_V\alpha_2\delta$ gabapentinoid binding site provides a platform to dissect the mechanisms by which these drugs affect Ca_V function and should guide the development of next-generation $\text{Ca}_V\alpha_2\delta$ -directed drugs for the treatment of pain and anxiety.

Online content

Any methods, additional references, Nature Portfolio reporting summaries, source data, extended data, supplementary information, acknowledgements, peer review information; details of author contributions and competing interests; and statements of data and code availability are available at <https://doi.org/10.1038/s41594-023-00951-7>.

Methods

Expression and purification of human $\text{Ca}_V1.2$

Expression and purification of $\text{Ca}_V1.2$ (C)/ $\text{Ca}_V\beta_3$ / $\text{Ca}_V\alpha_2\delta$ -1 was carried out, as previously described¹³ using an HEK293S GnTI⁻ (ATCC #CRL-3022) ‘ $\text{Ca}_V\beta_3$ -stable’ cell line expressing rabbit $\text{Ca}_V\beta_3$ (477 residues, UniProt P54286) bearing a Strep-tag II sequence³⁸. The codon-optimized construct of human $\text{Ca}_V1.2$ bore a C-terminal truncation at residue 1648 (denoted $\text{Ca}_V1.2$ (C)), a site located 13 residues after the end of the IQ domain (1649–2138, UniProt Q13936–20, 1,648 residues), followed by a 3C protease cleavage site, monomeric enhanced green fluorescent protein, and a His tag. The second construct carried unmodified rabbit $\text{Ca}_V\alpha_2\delta$ -1 (1,105 residues, UniProt P13806–1). Both constructs were cloned into modified pFastBac expression vectors having the polyhedrin promoter replaced by a mammalian cell active CMV promoter³⁹. All constructs were sequenced completely.

Chemically competent DH10EmBacY (Geneva Biotech) were used to generate the recombinant bacmid DNA, which was then used to transfect *Spodoptera frugiperda* (Sf9; Expression Systems, #94–001F) cells to make baculoviruses for each subunit⁴⁰. Ca_v1.2 was expressed in Ca_vβ₃-stable cells together with Ca_vα₂δ-1 using a baculovirus transduction-based system⁴⁰. Ca_vβ₃-stable cells were grown in suspension at 37 °C while supplied with 8% CO₂ in FreeStyle 293 Expression Medium (Gibco) supplemented with 2% fetal bovine serum (Peak Serum), and were transduced with 5% (vol/vol) baculovirus for each target subunit when the cell density reached ~2.5 × 10⁶ cells per ml. Sodium butyrate (10 mM) was added to the cell culture 16–24 h post-transduction, and the cells were subsequently grown at 30 °C. Cells were collected 48 h post-transduction by centrifugation at 5,000g for 30 min. The pellet was washed with Dulbecco's phosphate buffered saline (Gibco) and stored at –80 °C.

A cell pellet (from ~3.6 l of culture) was resuspended in 200 ml of resuspension buffer containing 0.3 M sucrose, 1 mM ethylenediaminetetraacetic acid, 10 mM Tris-HCl, pH 8.0 supplemented with 1 mM phenylmethylsulfonyl fluoride, and four Pierce protease inhibitor tablets (Thermo Scientific), then stirred gently on a Variomag magnetic stirrer (Mono Direct, Thermo Scientific) at 4 °C for 30 min. The membrane fraction was collected by centrifugation at 185,500g for 1 h and subsequently solubilized in 200 ml of solubilization buffer (buffer S) containing 500 mM NaCl, 5% glycerol (vol/vol), 0.5 mM CaCl₂, 20 mM Tris-HCl, pH 8.0, and supplemented with 1% (wt/vol) glycol-diosgenin (GDN) and rotated on an Orbitron rotator II (speed mode S; Boekel Scientific) at 4 °C for 2 h. The supernatant, collected by centrifugation at 185,500g for 1 h, was diluted with an equal volume of buffer S to a final concentration of 0.5% GDN and incubated with anti-GFP nanobody Sepharose resin⁴¹ at 4 °C overnight. The resin was loaded on an Econo-Column chromatography column (BioRad) and was then washed stepwise with 20 column volumes (CV) of buffer S supplemented with 0.1% (wt/vol) GDN, 20 CV of buffer S supplemented with 0.02% (wt/vol) GDN, and 20 CV of elution buffer (buffer E) containing 150 mM NaCl, 0.5 mM CaCl₂, 0.02% (wt/vol) GDN, 20 mM Tris-HCl pH 8.0. The protein was eluted with 3C protease⁴² and subsequently incubated at 4 °C for 2 h with 4 ml of *Strep*-tactin Superflow Plus beads (Qiagen) pre-equilibrated with buffer E. The beads were washed with 20 CV of buffer E, and the protein was eluted with buffer E supplemented with 2.5 mM desthiobiotin. The eluent was concentrated using an Amicon Ultra-15 100-kDa-cutoff centrifugal filter unit (Merck Millipore) before purification on a Superose 6 Increase 10/300 GL gel filtration column (GE Healthcare) pre-equilibrated in buffer E. Concentrated Ca_v1.2(C)/Ca_vβ₃/Ca_vα₂δ-1 sample was immediately incubated with GBP (final concentration 2 mg ml⁻¹, 11.7 mM; Sigma-Aldrich) on ice for 4 h before cryo-EM sample preparation, denoted Ca_v1.2(C)/Ca_vβ₃/Ca_vα₂δ-1:GBP.

Sample preparation and cryo-EM data acquisition

For cryo-EM, 3.5 μl of 2.0 mg ml⁻¹ Ca_v1.2(C)/Ca_vβ₃/Ca_vα₂δ-1:GBP was applied to Quantifoil R1.2/1.3 300 mesh Au holey-carbon grids, blotted for 4–6 s at 4 °C and 100% humidity using a FEI Vitrobot Mark IV (Thermo Fisher Scientific), and plunge-frozen in liquid ethane. The cryo-EM grids were screened on an FEI Talos Arctica cryo-TEM system (Thermo Fisher Scientific; at University of California, San Francisco (UCSF) EM Facility)

operated at 200 kV and equipped with a K3 direct detector camera (Gatan), and then imaged on a 300-kV FEI Titan Krios microscope (Thermo Fisher Scientific) with a K3 direct detector camera (Gatan; UCSF). Cryo-EM datasets were collected in super-resolution counting mode at a nominal magnification of $\times 105,000$ with a super-resolution pixel size of 0.4175 Å (physical pixel size of 0.835 Å) using a SerialEM v4.1 (ref. 43). Images were recorded with a 2.024-s exposure over 81 frames with a dose rate of 0.57 e⁻ Å⁻² per frame. The defocus range was set from -0.9 μm to -1.7 μm.

Image processing and 3D reconstruction

A total of 26,928 movies were collected for Ca_v1.2(C)/Ca_vβ₃/Ca_vα₂δ-1:GBP. Initial image processing was carried out in cryoSPARC-3.3⁴⁴. Raw movies were corrected for motion and Fourier binned by a factor of two (final pixel size of 0.834 Å) with the patch motion correction program. Contrast transfer function parameters of the resulting micrographs were estimated with the Patch contrast transfer function estimation program in cryoSPARC-3.3. Particles were picked by blob picking, extracted using a box size of 440 pixel (2× binned to 220 pixels), and 2D-classified using a circular mask diameter of 260 Å. Selected particles represented by good 2D classes were subjected to one round of ab initio reconstruction and heterogeneous refinement with C1 symmetry. Particles having reasonable 3D reconstructions (as judged by the Fourier shell correlation (FSC) curve) were re-extracted to physical pixel size and subjected to iterative rounds of ab initio reconstruction and heterogeneous refinement. Further, non-uniform refinements were performed to achieve high-resolution reconstruction.

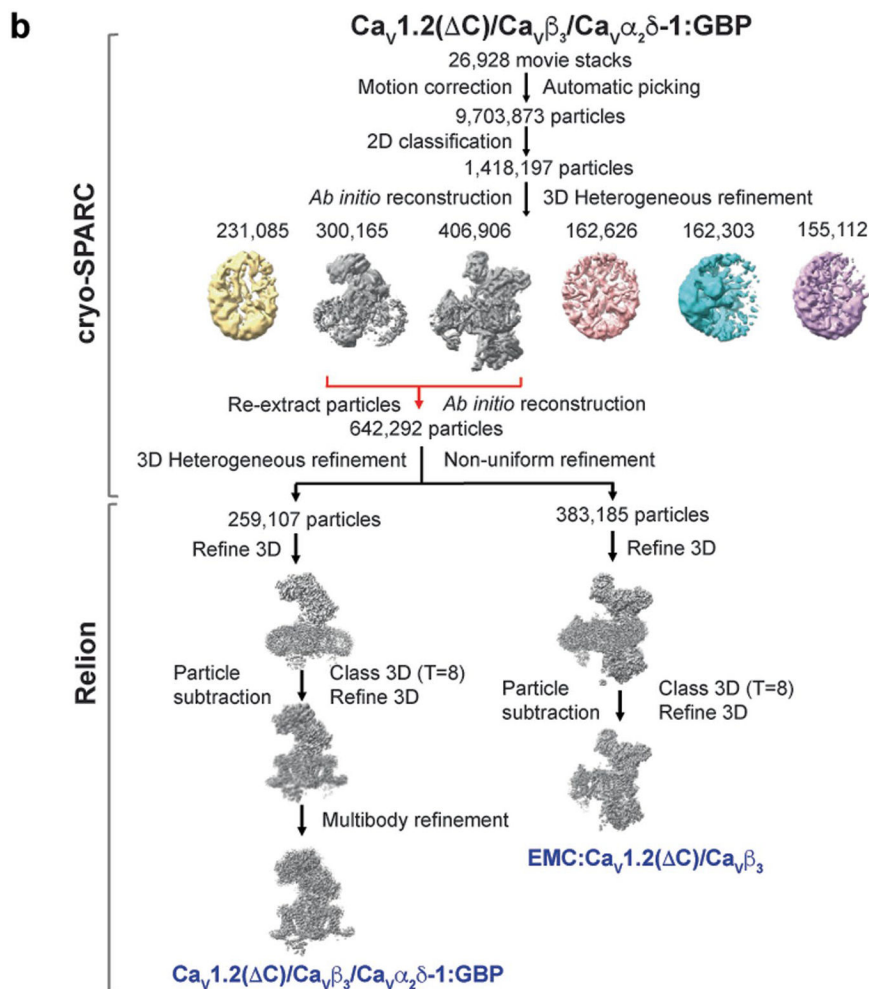
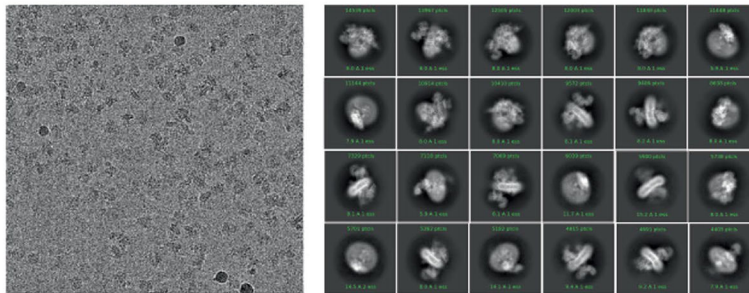
To improve the Ca_vα₂δ-1 3D reconstruction, multibody refinement was carried out in RELION-3.1⁴⁵. In total, 259,107 refined particles for the Ca_v1.2(C)/Ca_vβ₃/Ca_vα₂δ-1:GBP complex were exported from cryoSPARC-3.3 to RELION-3.1 using the csparc2star.py (UCSF pyem v0.5, Zenodo) suite of conversion scripts (<https://doi.org/10.5281/zenodo.3576630>). Following a 3D refinement in RELION-3.1 using the refined map from cryoSPARC-3.3 and the exported particles, an overall 3.1-Å EM density map (consensus map) was obtained (Extended Data Fig. 1 presents processing flow charts). Multibody refinement was performed in RELION-3.1 to improve the features of the luminal domain and the transmembrane region for the Ca_v1.2(C)/Ca_vβ₃/Ca_vα₂δ-1:GBP complex. We used the phenix.combine_focused_maps program to combine the improved features of the segments from multibody refinement and those of the consensus map to obtain the final map with best features for the Ca_v1.2(C)/Ca_vβ₃/Ca_vα₂δ-1:GBP complex⁴⁶.

As with an earlier report¹³, purification of Ca_v1.2(C)/Ca_vβ₃/Ca_vα₂δ-1 yielded a sample that also had a substantial portions of particles (383,185 refined particles) comprising the EMC:Ca_v1.2(C)/Ca_vβ₃ complex. These refined particles were exported from cryoSPARC-3.3 to RELION-3.1, and subsequent 3D refinement resulted in a 3.1-Å consensus map. Comparison of this 3.1-Å consensus map for the EMC:Ca_v1.2(C)/Ca_vβ₃ complex with the one reported from the previous study¹³ revealed no apparent conformational difference (cross correlation = 0.9554), so the model was not docked for this complex.

Model building and refinement

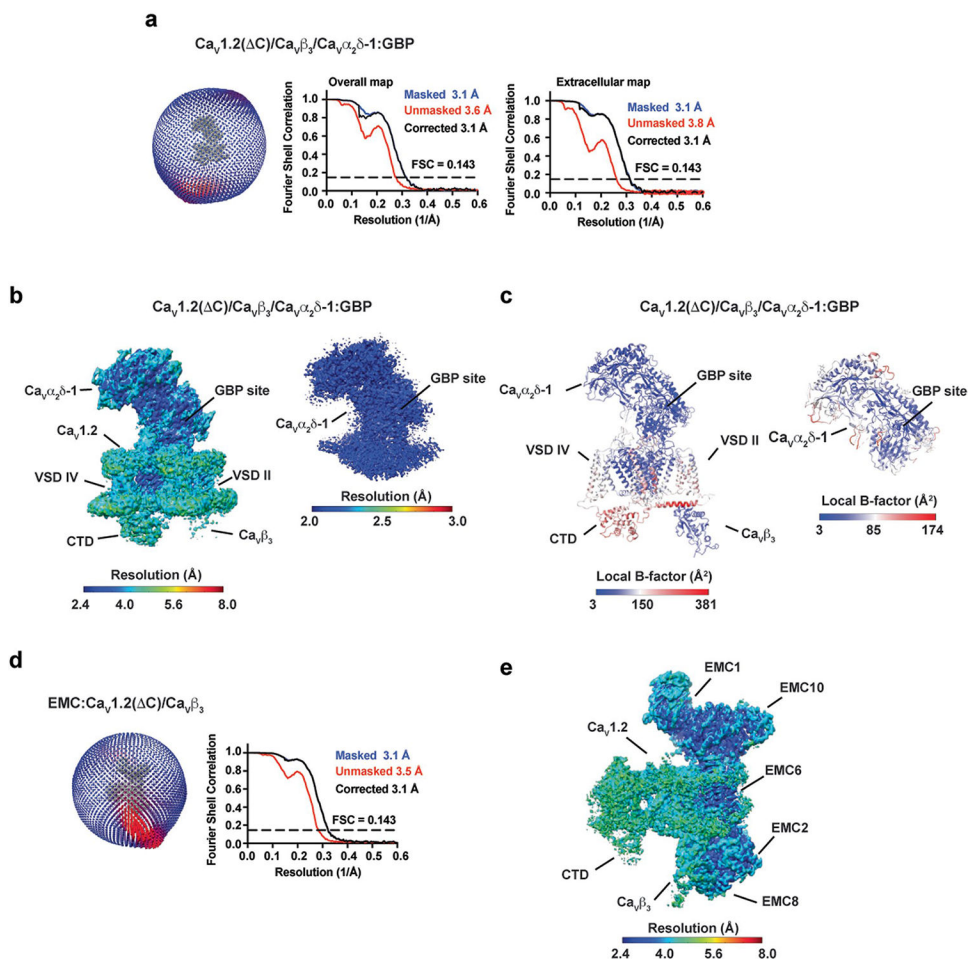
We used phenix.dock_in_map⁴⁶ to dock the Ca_v1.2(C)/Ca_vβ₃/Ca_vα₂δ-1 model (PDB 8EOG) into the Ca_v1.2(C)/Ca_vβ₃/Ca_vα₂δ-1:GBP map. As the density for Ca_vβ₃ was weaker than for other parts of the channel, we rendered the Ca_vβ region of the Ca_v1.2(C)/Ca_vβ₃/Ca_vα₂δ-1 complex at a threshold of 2.25 (>5 was used for the rest of map) and placed Ca_vβ₃ from the de novo modeled EMC:Ca_v1.2(C)/Ca_vβ₃ structure (EMD-28376; PDB 8EOI) in the density, followed by rigid-body refinement of the Ca_v1.2(C)/Ca_vβ₃/Ca_vα₂δ-1 complex. The docked model and maps were manually checked and fitted in Coot⁴⁷. Iterative structure refinement and model building were performed using the phenix.real_space_refine program⁴⁶. Restraint files necessary for refinement were generated using phenix.elbow^{46,48}. The final statistics of 3D reconstruction and model refinement are provided in Table 1. The per-residue *B* factors, after final refinement against the overall map, were rendered on the refined model and are presented in Extended Data Fig. 2c. The final models were evaluated using MolProbity⁴⁹. All figures and movies were generated using ChimeraX⁵⁰ and the Pymol package (v2.4.0; <http://www.pymol.org/pymol>). Close-contact interaction analyses were performed using LIGPLOT and DIMPLOT^{37,51}.

Extended Data

a $\text{Ca}_v1.2(\Delta\text{C})/\text{Ca}_v\beta_3/\text{Ca}_v\alpha_2\delta\text{-1:GBP}$ **Extended Data Fig. 1 | Ca_v1.2(C)/Ca_vβ₃/Ca_vα₂δ-1:GBP Cryo-EM analysis.**

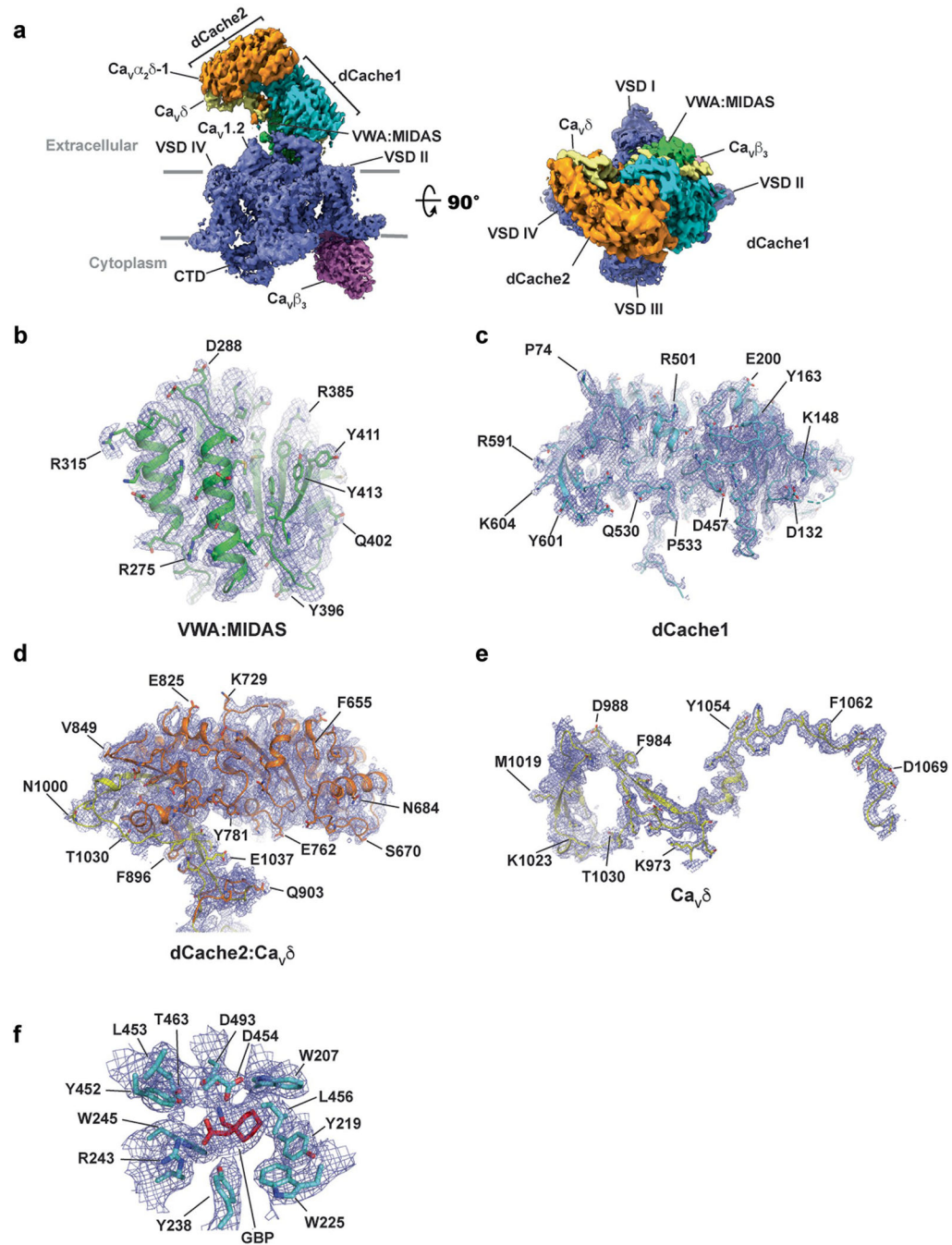
a, Exemplar $\text{Ca}_v1.2(\text{ C})/\text{Ca}_v\beta_3/\text{Ca}_v\alpha_2\delta\text{-1:GBP}$ electron micrograph ($\sim 105,000\times$ magnification) and 2D class averages. $N = 3$. **b**, Workflow for electron microscopy data processing for $\text{Ca}_v1.2(\text{ C})/\text{Ca}_v\beta_3/\text{Ca}_v\alpha_2\delta\text{-1:GBP}$ sample. Initial cryoSPARC-3.2 *Ab initio* reconstruction identified a population of particles containing the $\text{Ca}_v1.2(\text{ C})/\text{Ca}_v\beta_3/\text{Ca}_v\alpha_2\delta\text{-1}$ and EMC: $\text{Ca}_v1.2(\text{ C})/\text{Ca}_v\beta_3$ complexes, similar to prior studies¹³. Red arrows indicate the two classes that were re-extracted, subjected to multiple rounds of 3D

heterogeneous classification, and exported from cryoSPARC-3.2 for further 3D refinement in RELION-3.1. Particle subtraction was performed for both the refined maps in Relion-3.1 followed by 3D classification with single class and 3D refinement to get the final consensus maps. Multibody refinement was performed to enhance features of $\text{Ca}_v\alpha_2\delta-1$, which was used for the $\text{Ca}_v1.2(\text{C})/\text{Ca}_v\beta_3/\text{Ca}_v\alpha_2\delta-1:\text{GBP}$ composite map. The composite map was used for model building and refinement.



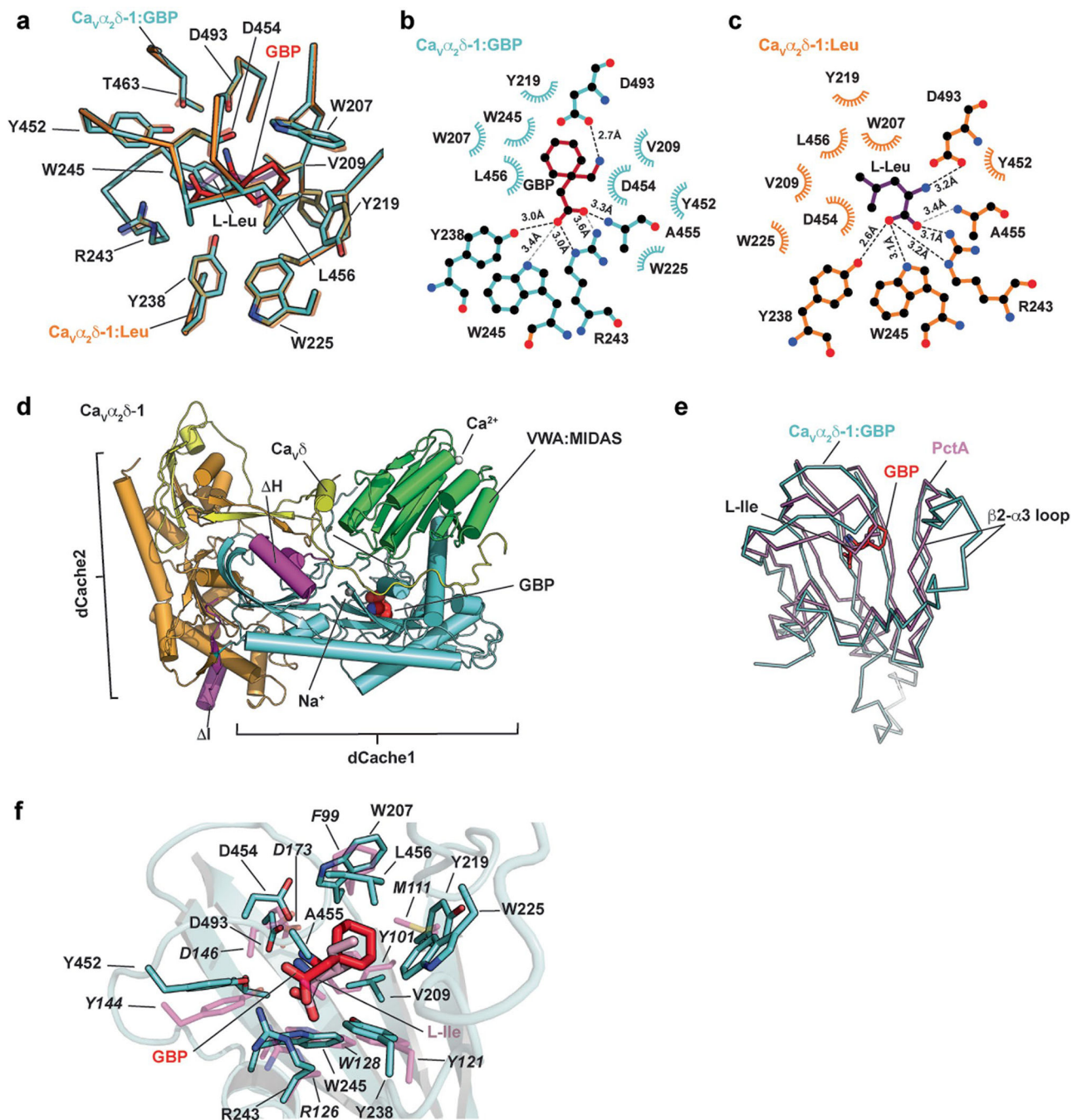
Extended Data Fig. 2 | $\text{Ca}_v1.2(\text{C})/\text{Ca}_v\beta_3/\text{Ca}_v\alpha_2\delta-1:\text{GBP}$ map and model quality.

a, Particle distribution plot and gold-standard Fourier shell correlation (FSC) curve for the overall $\text{Ca}_v1.2(\text{C})/\text{Ca}_v\beta_3/\text{Ca}_v\alpha_2\delta-1:\text{GBP}$ complex map and the extracellular map containing $\text{Ca}_v\alpha_2\delta-1:\text{GBP}$. **b**, local resolution for the overall $\text{Ca}_v1.2(\text{C})/\text{Ca}_v\beta_3/\text{Ca}_v\alpha_2\delta-1:\text{GBP}$ map and the extracellular map containing $\text{Ca}_v\alpha_2\delta-1:\text{GBP}$. **c**, local B-factor for the overall $\text{Ca}_v1.2(\text{C})/\text{Ca}_v\beta_3/\text{Ca}_v\alpha_2\delta-1:\text{GBP}$ model and the $\text{Ca}_v\alpha_2\delta-1:\text{GBP}$ subunit. **d**, Particle distribution plot and gold-standard Fourier shell correlation (FSC) curve for the EMC: $\text{Ca}_v1.2(\text{C})/\text{Ca}_v\beta_3$ complex from the $\text{Ca}_v1.2(\text{C})/\text{Ca}_v\beta_3/\text{Ca}_v\alpha_2\delta-1:\text{GBP}$ sample. **e**, EMC: $\text{Ca}_v1.2(\text{C})/\text{Ca}_v\beta_3$ complex local resolution. Select elements of each complex are labeled.



Extended Data Fig. 3 | Ca_v1.2(C)/Ca_vβ₃/Ca_vα₂δ-1:GBP Cryo-EM maps.

a, Ca_v1.2(C)/Ca_vβ₃/Ca_vα₂δ-1 side view (left) and extracellular (right) view. Subunits are colored: Ca_v1.2 (slate) and Ca_vβ₃ (violet). Ca_vα₂δ domains are colored as: dCache1 (aquamarine), dCache2 (orange), VWA:MIDAS (green), and Ca_vδ (yellow). Grey bars denote the membrane. **b-e**, Ca_vα₂δ-1 subdomain representative maps for **b**, VWA:MIDAS domain, **c**, dCache1, **d**, dCache2:Ca_vδ. Part of Ca_vδ completes the second β-barrel subdomain of dCache2, **e**, Ca_vδ. **f**, GBP-binding site. Maps are rendered at 9–10σ. Domain colors are as in **a**.



Extended Data Fig. 4 | $Ca_v\alpha_2\delta-1$ GBP-binding site analysis and comparisons.

a, Superposition of the $Ca_v\alpha_2\delta-1:GBP$ (aquamarine) and $Ca_v\alpha_2\delta-1:L-Leu$ (PDB:8EOG)¹³ binding sites. GBP is red. L-Leu is purple. **b** and **c**, LigPLOT³⁷ diagrams of the **b**, $Ca_v\alpha_2\delta-1:GBP$ (aquamarine) and **c**, $Ca_v\alpha_2\delta-1:L-Leu$ (PDB:8EOG)¹³ binding sites showing hydrogen bonds and ionic interactions (dashed lines) and van der Waals contacts ≤ 5 Å. GBP is red. L-Leu is purple. **d**, Superposition of the first dCache1 repeats from $Ca_v\alpha_2\delta-1:GBP$ (aquamarine) and the PctA:L-Ile complex (magenta) (PDB: 5T65)³⁴. GBP is red. **e,f**, Closeup view of superposition from 'd' showing ligand contact

residues. $\text{Ca}_v\alpha_2\delta-1$ is shown as a cartoon. GBP is red. Corresponding sidechains of PctA are magenta. L-Ile from the PctA complex is pink. PctA residues are labeled in italics.

Supplementary Material

Refer to Web version on PubMed Central for supplementary material.

Acknowledgements

We thank D. Bulkley for technical help and K. Brejc for comments on the manuscript. This work was supported by grant no. NIH R01 HL080050 to D.L.M.

Data availability

$\text{Ca}_v1.2(\text{C})/\text{Ca}_v\beta_3/\text{Ca}_v\alpha_2\delta-1$:GBP coordinates and maps (PDB 8FD7, EMD-29004, EMD-29007 and EMD-29015) and the map of the EMC: $\text{Ca}_v1.2(\text{C})/\text{Ca}_v\beta_3$ complex (EMD-29006) are deposited with the RCSB and EMDB. Requests for materials should be addressed to D.L.M.

References

1. Dooley DJ, Taylor CP, Donevan S & Feltner D Ca^{2+} channel $\alpha_2\delta$ ligands: novel modulators of neurotransmission. *Trends Pharmacol. Sci.* 28, 75–82 (2007). [PubMed: 17222465]
2. Taylor CP, Angelotti T & Fauman E Pharmacology and mechanism of action of pregabalin: the calcium channel $\alpha_2\delta$ ($\alpha_2\delta$) subunit as a target for antiepileptic drug discovery. *Epilepsy Res.* 73, 137–150 (2007). [PubMed: 17126531]
3. Field MJ et al. Identification of the $\alpha_2\delta-1$ subunit of voltage-dependent calcium channels as a molecular target for pain mediating the analgesic actions of pregabalin. *Proc. Natl Acad. Sci. USA* 103, 17537–17542 (2006). [PubMed: 17088553]
4. Domon Y et al. Binding characteristics and analgesic effects of Mirogabalin, a novel ligand for the $\alpha_2\delta$ subunit of voltage-gated calcium channels. *J. Pharmacol. Exp. Ther.* 365, 573–582 (2018). [PubMed: 29563324]
5. Kato J, Inoue T, Yokoyama M & Kuroha M A review of a new voltage-gated Ca^{2+} channel $\alpha_2\delta$ ligand, mirogabalin, for the treatment of peripheral neuropathic pain. *Expert Opin. Pharmacother.* 22, 2311–2322 (2021). [PubMed: 34431423]
6. Gee NS et al. The novel anticonvulsant drug, gabapentin (Neurontin), binds to the $\alpha_2\delta$ subunit of a calcium channel. *J. Biol. Chem.* 271, 5768–5776 (1996). [PubMed: 8621444]
7. Bauer CS et al. The increased trafficking of the calcium channel subunit $\alpha_2\delta-1$ to presynaptic terminals in neuropathic pain is inhibited by the $\alpha_2\delta$ ligand pregabalin. *J. Neurosci.* 29, 4076–4088 (2009). [PubMed: 19339603]
8. Cassidy JS, Ferron L, Kadurin I, Pratt WS & Dolphin AC Functional exofacially tagged N-type calcium channels elucidate the interaction with auxiliary $\alpha_2\delta-1$ subunits. *Proc. Natl Acad. Sci. USA* 111, 8979–8984 (2014). [PubMed: 24889613]
9. Marais E, Klugbauer N & Hofmann F Calcium channel $\alpha_2\delta$ subunits-structure and Gabapentin binding. *Mol. Pharmacol.* 59, 1243–1248 (2001). [PubMed: 11306709]
10. Qin N, Yagel S, Momplaisir ML, Codd EE & D'Andrea MR Molecular cloning and characterization of the human voltage-gated calcium channel $\alpha_2\delta-4$ subunit. *Mol. Pharmacol.* 62, 485–496 (2002). [PubMed: 12181424]
11. Meyer JO & Dolphin AC Rab11-dependent recycling of calcium channels is mediated by auxiliary subunit $\alpha_2\delta-1$ but not $\alpha_2\delta-3$. *Sci. Rep.* 11, 10256 (2021). [PubMed: 33986433]

12. Tran-Van-Minh A & Dolphin AC The $\alpha_2\delta$ ligand gabapentin inhibits the Rab11-dependent recycling of the calcium channel subunit $\alpha_2\delta$ -2. *J. Neurosci.* 30, 12856–12867 (2010). [PubMed: 20861389]
13. Chen Z et al. EMC holdase:Ca ν 1.2/Ca ν β 3 complex and Ca ν 1.2 channel structures reveal Ca ν assembly and drug binding mechanisms. Preprint at bioRxiv 10.1101/2022.10.03.510667 (2022).
14. Zamponi GW, Striessnig J, Koschak A & Dolphin AC The physiology, pathology and pharmacology of voltage-gated calcium channels and their future therapeutic potential. *Pharm. Rev.* 67, 821–870 (2015). [PubMed: 26362469]
15. Nanou E & Catterall WA Calcium channels, synaptic plasticity and neuropsychiatric disease. *Neuron* 98, 466–481 (2018). [PubMed: 29723500]
16. Buraei Z & Yang J The β subunit of voltage-gated Ca $^{2+}$ channels. *Physiol. Rev.* 90, 1461–1506 (2010). [PubMed: 20959621]
17. Dolphin AC Voltage-gated calcium channels and their auxiliary subunits: physiology and pathophysiology and pharmacology. *J. Physiol.* 594, 5369–5390 (2016). [PubMed: 27273705]
18. Brown JP, Dissanayake VU, Briggs AR, Milic MR & Gee NS Isolation of the [3 H]gabapentin-binding protein/ $\alpha_2\delta$ Ca $^{2+}$ channel subunit from porcine brain: development of a radioligand binding assay for $\alpha_2\delta$ subunits using [3 H]leucine. *Anal. Biochem.* 255, 236–243 (1998). [PubMed: 9451509]
19. Dolphin AC Calcium channel auxiliary $\alpha_2\delta$ and β subunits: trafficking and one step beyond. *Nat. Rev. Neurosci.* 13, 542–555 (2012). [PubMed: 22805911]
20. David DJ, Donovan CM, Meder WP & Whetzel SZ Preferential action of gabapentin and pregabalin at P/Q-type voltage-sensitive calcium channels: inhibition of K $^+$ -evoked [3 H]-norepinephrine release from rat neocortical slices. *Synapse* 45, 171–190 (2002). [PubMed: 12112396]
21. Anantharaman V & Aravind L Cache—a signaling domain common to animal Ca $^{2+}$ -channel subunits and a class of prokaryotic chemotaxis receptors. *Trends Biochem. Sci.* 25, 535–537 (2000). [PubMed: 11084361]
22. Jonikas MC et al. Comprehensive characterization of genes required for protein folding in the endoplasmic reticulum. *Science* 323, 1693–1697 (2009). [PubMed: 19325107]
23. Christianson JC et al. Defining human ERAD networks through an integrative mapping strategy. *Nat. Cell Biol.* 14, 93–105 (2011). [PubMed: 22119785]
24. Hegde RS The function, structure, and origins of the ER membrane protein complex. *Annu. Rev. Biochem.* 91, 651–678 (2022). [PubMed: 35287476]
25. Wu J et al. Structure of the voltage-gated calcium channel Ca ν 1.1 at 3.6 Å resolution. *Nature* 537, 191–196 (2016). [PubMed: 27580036]
26. Yao X, Gao S & Yan N Structural basis for pore blockade of human voltage-gated calcium channel Ca ν 1.3 by motion sickness drug cinnarizine. *Cell Res.* 32, 946–948 (2022). [PubMed: 35477996]
27. Gao S, Yao X & Yan N Structure of human Ca ν 2.2 channel blocked by the painkiller ziconotide. *Nature* 596, 143–147 (2021). [PubMed: 34234349]
28. Gumerov VM et al. Amino acid sensor conserved from bacteria to humans. *Proc. Natl Acad. Sci. USA* 119, e2110415119 (2022). [PubMed: 35238638]
29. Canti C et al. The metal-ion-dependent adhesion site in the von Willebrand factor-A domain of $\alpha_2\delta$ subunits is key to trafficking voltage-gated Ca $^{2+}$ channels. *Proc. Natl Acad. Sci. USA* 102, 11230–11235 (2005). [PubMed: 16061813]
30. Wang M, Offord J, Oxender DL & Su TZ Structural requirement of the calcium-channel subunit $\alpha_2\delta$ for gabapentin binding. *Biochem. J.* 342, 313–320 (1999). [PubMed: 10455017]
31. Oyama M, Watanabe S, Iwai T & Tanabe M Mirogabalin activates the descending noradrenergic system by binding to the $\alpha_2\delta$ -1 subunit of voltage-gated Ca $^{2+}$ channels to generate analgesic effects. *J. Pharm. Sci.* 146, 33–39 (2021).
32. Lotarski S et al. Anticonvulsant activity of pregabalin in the maximal electroshock-induced seizure assay in $\alpha_2\delta_1$ (R217A) and $\alpha_2\delta_2$ (R279A) mouse mutants. *Epilepsy Res.* 108, 833–842 (2014). [PubMed: 24698052]

33. Lotarski SM et al. Anxiolytic-like activity of pregabalin in the Vogel conflict test in $\alpha_2\delta$ -1 (R217A) and $\alpha_2\delta$ -2 (R279A) mouse mutants. *J. Pharmacol. Exp. Ther.* 338, 615–621 (2011). [PubMed: 21558437]
34. Gavira JA et al. How bacterial chemoreceptors evolve novel ligand specificities. *mBio* 10.1128/mBio.03066-19 (2020).
35. Page KM, Gumerov VM, Dahimene S, Zhulin IB & Dolphin AC The importance of cache domains in $\alpha_2\delta$ proteins and the basis for their gabapentinoid selectivity. *Channels (Austin)* 17, 2167563 (2023). [PubMed: 36735378]
36. Dahimene S et al. The $\alpha_2\delta$ -like protein Cachd1 increases N-type calcium currents and cell surface expression and competes with $\alpha_2\delta$ -1. *Cell Rep.* 25, 1610–1621 (2018). [PubMed: 30404013]

References

37. Wallace AC, Laskowski RA & Thornton JM LIGPLOT: a program to generate schematic diagrams of protein-ligand interactions. *Protein Eng.* 8, 127–134 (1995). [PubMed: 7630882]
38. Schmidt TG & Skerra A The Strep-tag system for one-step purification and high-affinity detection or capturing of proteins. *Nat. Protoc.* 2, 1528–1535 (2007). [PubMed: 17571060]
39. Liao M, Cao E, Julius D & Cheng Y Structure of the TRPV1 ion channel determined by electron cryo-microscopy. *Nature* 504, 107–112 (2013). [PubMed: 24305160]
40. Goehring A et al. Screening and large-scale expression of membrane proteins in mammalian cells for structural studies. *Nat. Protoc.* 9, 2574–2585 (2014). [PubMed: 25299155]
41. Lee H, Lolicato M, Arrigoni C & Minor DL Jr Production of K2P2.1 (TREK-1) for structural studies. *Methods Enzymol.* 653, 151–188 (2021). [PubMed: 34099170]
42. Shaya D et al. Voltage-gated sodium channel (NaV) protein dissection creates a set of functional pore-only proteins. *Proc. Natl Acad. Sci. USA* 108, 12313–12318 (2011). [PubMed: 21746903]
43. Mastronarde DN Automated electron microscope tomography using robust prediction of specimen movements. *J. Struct. Biol.* 152, 36–51 (2005). [PubMed: 16182563]
44. Punjani A, Rubinstein JL, Fleet DJ & Brubaker MA cryoSPARC: algorithms for rapid unsupervised cryo-EM structure determination. *Nat. Methods* 14, 290–296 (2017). [PubMed: 28165473]
45. Zivanov J et al. New tools for automated high-resolution cryo-EM structure determination in RELION-3. *eLife* 7, e42166 (2018). [PubMed: 30412051]
46. Liebschner D et al. Macromolecular structure determination using X-rays, neutrons and electrons: recent developments in Phenix. *Acta Crystallogr. D Struct. Biol.* 75, 861–877 (2019).
47. Emsley P, Lohkamp B, Scott WG & Cowtan K Features and development of Coot. *Acta Crystallogr. D* 66, 486–501 (2010). [PubMed: 20383002]
48. Moriarty NW, Grosse-Kunstleve RW & Adams PD Electronic Ligand Builder and Optimization Workbench (eLBOW): a tool for ligand coordinate and restraint generation. *Acta Crystallogr. D* 65, 1074–1080 (2009). [PubMed: 19770504]
49. Williams CJ et al. MolProbity: more and better reference data for improved all-atom structure validation. *Protein Sci.* 27, 293–315 (2018). [PubMed: 29067766]
50. Pettersen EF et al. UCSF ChimeraX: structure visualization for researchers, educators and developers. *Protein Sci.* 30, 70–82 (2021). [PubMed: 32881101]
51. Laskowski RA & Swindells MB LigPlot+: multiple ligand-protein interaction diagrams for drug discovery. *J. Chem. Inf. Model.* 51, 2778–2786 (2011). [PubMed: 21919503]

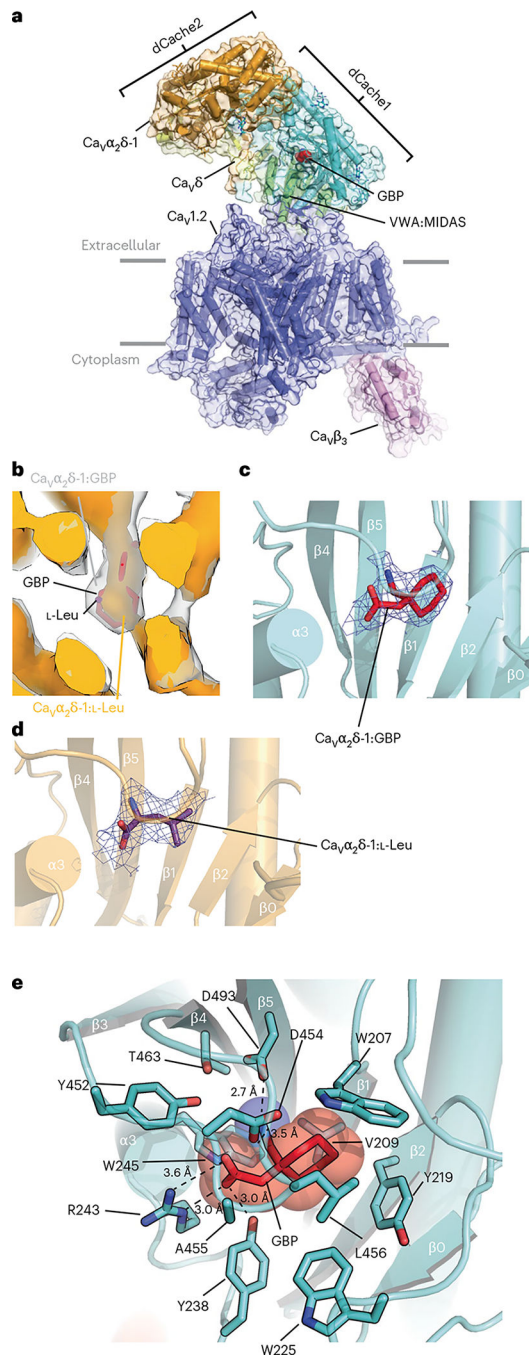


Fig. 1 | Structure of the $\text{Ca}_V1.2(\text{C})/\text{Ca}_V\beta_3/\text{Ca}_V\alpha_2\delta-1:\text{GBP}$ complex.

a, Side view of the $\text{Ca}_V1.2(\text{C})/\text{Ca}_V\beta_3/\text{Ca}_V\alpha_2\delta-1:\text{GBP}$ complex. Subunits are colored with $\text{Ca}_V1.2(\text{C})$ in slate and $\text{Ca}_V\beta_3$ in violet. $\text{Ca}_V\alpha_2\delta$ domains are colored with dCache1 in aquamarine, dCache2 in orange, VWA:MIDAS in green and $\text{Ca}_V\delta$ in yellow. GBP (in red) is shown as space filling. Gray bars denote the membrane. **b**, Comparison of $\text{Ca}_V\alpha_2\delta-1$ dCache1 binding sites. Map comparison of the dCache1 ligand-binding site for the GBP complex (clear) and the L-Leu complex¹³ (orange). GBP is shown as red sticks. Map label colors match the respective map colors. **c,d**, Ligand densities for GBP (10 σ , red, **c**) and

L-Leu (7σ , violet purple, **d**) in the dCache1 domains are shown as cartoons (aquamarine and light orange, respectively). **e**, Ca ν $\alpha_2\delta$ -1 dCache1 ligand-binding site details. GBP (red) and contacting Ca ν $\alpha_2\delta$ -1 side chains (green-cyan) are shown as sticks. Distances for the dashed-line interactions are indicated.

Author Manuscript

Author Manuscript

Author Manuscript

Author Manuscript

Table 1

Statistics for data collection, refinement and validation

	Cav1.2(C)/Cav β_3 /Cav $\alpha_2\delta$ -1:GBP
Data collection and processing	
Magnification	105,000
Voltage (kV)	300
Electron dose (e ⁻ /Å ²)	46
Defocus range (μm)	-0.9~--1.7
Pixel size (Å)	0.835
Symmetry	C1
Initial particle images (no.)	9,703,873
	Cav1.2(C)/Cav β_3 /Cav $\alpha_2\delta$ -1:GBP (PDB 8FD7; EMD-29004) EMC:Cav1.2(C)/Cav β_3 (EMD-29006)
Final particle images (no.)	259,107
Map resolution (Å)	3.1
FSC threshold	0.143
Map resolution range (Å)	~2.4–8.0
	~2.4–8.0
Refinement	
Initial model used (PDB code)	8EOG
Model resolution (Å)	3.3
FSC threshold	0.5
Map sharpening <i>B</i> factor (Å ²)	-20
Model composition	
Nonhydrogen atoms	19,701
Protein residues	2,416
Ligands	20
<i>B</i> factors (Å ²)	
Protein	118.63
Ligand	42.23
r.m.s. deviations	

Author Manuscript

Author Manuscript

Author Manuscript

Author Manuscript

	Cav1.2(C)/Cavβ3/Cavα2δ-1:GBP
Bond lengths (Å)	0.002
Bond angles (°)	0.479
Validation	
MolProbity score	2.16
Clashscore	7.54
Rotamer outliers (%)	2.76
Ramachandran plot	
Favored (%)	93.78
Allowed (%)	6.10
Outliers (%)	0.13